Medical Image Analysis 33 (2016) 165–169

Contents lists available at ScienceDirect

Medical Image Analysis

journal homepage: www.elsevier.com/locate/media

Editorial

Quantitative analysis of retinal OCT

Milan Sonka[a,b,c,*], Michael D. Abràmoff[a,b,c]

[a] Iowa Institute for Biomedical Imaging, The University of Iowa, Iowa City, IA 52242, United States
[b] Department of Ophthalmology & Visual Sciences, The University of Iowa, Iowa City, IA 52242, United States
[c] Department of Electrical & Computer Engineering, The University of Iowa, Iowa City, IA 52242, United States

ARTICLE INFO

Article history:
Received 30 March 2016
Revised 22 May 2016
Accepted 6 June 2016
Available online 12 July 2016

Keywords:
Quantitative medical imaging
Optical coherence tomography (OCT)
Retina
Choroid
Visual function
LOGISMOS

ABSTRACT

Clinical acceptance of 3-D OCT retinal imaging brought rapid development of quantitative 3-D analysis of retinal layers, vasculature, retinal lesions as well as facilitated new research in retinal diseases. One of the cornerstones of many such analyses is segmentation and thickness quantification of retinal layers and the choroid, with an inherently 3-D simultaneous multi-layer LOGISMOS (Layered Optimal Graph Image Segmentation for Multiple Objects and Surfaces) segmentation approach being extremely well suited for the task. Once retinal layers are segmented, regional thickness, brightness, or texture-based indices of individual layers can be easily determined and thus contribute to our understanding of retinal or optic nerve head (ONH) disease processes and can be employed for determination of disease status, treatment responses, visual function, etc. Out of many applications, examples provided in this paper focus on image-guided therapy and outcome prediction in age-related macular degeneration and on assessing visual function from retinal layer structure in glaucoma.

1. Introduction

Many eye diseases and a number of systemic diseases of the brain, cardiovascular system, and others manifest themselves in the retina. Examples include diabetes mellitus and its most feared complication diabetic retinopathy, age-related macular degeneration, glaucoma, and an entire barrage of cardiovascular diseases. The retina has traditionally been imaged using 2-D fundus photography, a technique tracing its origin to the discovery of the first ophthalmoscope by Purkyne˘ in 1823 and its reinvention by Babbage in 1845. With the introduction of 3-D retinal imaging based on the principle of optical coherence tomography and its wide clinical acceptance in the early years of the 21st century, quantitative 3-D analysis of retinal layers, vasculature, as well as volumetric analysis of retinal lesions became possible, at a resolution approaching that of individual cells, and at minimal patient risk or inconvenience. This move to high resolution 3-D happened at least 2–3 decades after 3-D image datasets started to be available in radiology from X-ray CT, MRI, and other medical imaging modalities. The greatest advantage of this delay was the readiness of the quantitative medical imaging community to immediately start developing truly three-dimensional image analysis approaches. Due to many years of experience with 3-D CT, MR, and ultrasound image datasets, the progress has been fast, a number of quantitative techniques were developed quickly, and became available for routine quantitative measurements on relatively inexpensive retinal OCT scanners, inexpensive at least in comparison with CT, MR, PET and other radiologic imaging scanners (Abràmoff et al., 2010). The brief sections below outline a small subset of methods and disease-specific results achieved in the Iowa Institute for Biomedical Imaging at the University of Iowa over the past decade or so, combining some of the most sophisticated 3-D/4-D image analysis approaches with the ophthalmologists' desire for improvements in precision medicine and patient-specific treatments via screening, quantification, outcome prediction, and image guided therapy.

2. Retinal OCT

The principle of Optical Coherence Tomography (OCT) is the estimation of the depth at which a specific backscatter originated by measuring its time of flight. Backscatters are typically caused by refractive index transitions from one tissue to an-other. The backscatter from deeper tissues can be differentiated from backscatter originating at more superficial tissues because it takes longer for the light to arrive at the sensor. As the total retinal thickness is 300–500 μm, the differences in time of flight are very small and can only be measured through interferometry. OCT employs low-coherent light interferometry–while the wavelengths used for OCT are typically slightly longer than visible light in order to allow resolving deeper retinal layers and increase patient comfort. For 3-D imaging, the illuminating beam is typically moved

* Corresponding author. Fax: 1 (319)335 6028.
E-mail address: milan-sonka@uiowa.edu (M. Sonka).

http://dx.doi.org/10.1016/j.media.2016.06.001
1361-8415/

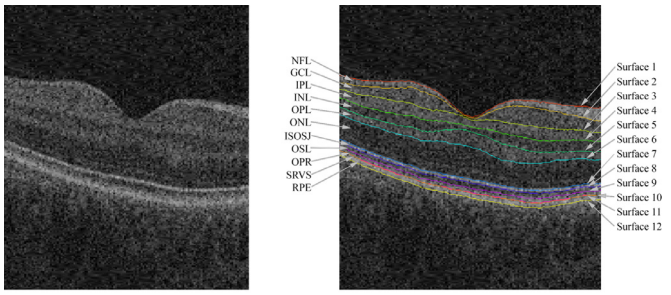

Fig. 1. Segmentation results of 12 retinal surfaces (11 layers). (a) X-Z image of the OCT volume. (b) Segmentation results, nerve fiber layer (NFL), ganglion cell layer (GCL), inner plexiform layer (IPL), inner nuclear layer (INL), outer plexiform layer (OPL), outer nuclear layer (ONL), inner segment outer segment junction (ISOSJ), outer segment layer (OSL), Outer segment photoreceptors (OPR), subretinal virtual space (SRVS–zero thickness in normals), and retinal pigment epithelium (RPE). The stated anatomical labeling is based on observed relationships with histology although no general agreement exists among experts about precise correspondence of some layers, especially the outermost layers.

across the retina in a row-by-column manner, resulting in a tomographic image with an A-scan for each x; y location. Currently, hundreds of thousands of A-scans can be obtained in a second, bringing increase in image resolution and decreases in scanning time on a regular basis. The most frequently used OCT scanners cover a 20° retinal field or the retinal area of $6 \times 6\text{mm}^2$ (Fig. 1a). The most recent "wide-field" OCT scanners image a wider area of the retina, with a 40° imaging angle and retinal coverage of $12 \times 9\text{mm}^2$. The used OCT wavelength typically ranges from 860 to 1000 μm, with longer wavelengths allowing deeper tissue penetration and shorter wavelengths offering higher resolution along each A-scan. If a larger area of the retina needs to be imaged, coverage can be achieved by stitching (registering) several partly overlapping OCT fields acquired in a sequential manner. By repeat imaging of the same location, and analyzing local changes of intensity, so called OCT angiography allows moving blood to be imaged. OCT scanners allow to combine the ability to identify vascular pattern with the ability to repeatedly image the same retinal location, resulting in visually pleasing lower noise images obtained from temporal averaging of multiple co-located B-scans (Geitzenauer et al., 2011).

3. Segmentation and quantification of retinal layers

Once the volumetric OCT image of the retina is formed, retinal layers coinciding with specific cellular layers are clearly visible–see Fig. 1a. Since thinning or thickening of individual layers may be indicators of retinal diseases or precursors of future visual loss, segmentation of individual layers and location-specific quantification of their thicknesses is of major clinical relevance. Considering the multi-layer appearance and volumetric character of retinal OCT scans, our multi-surface multi-object LOGISMOS (Layered Optimal Graph Image Segmentation for Multiple Objects and Surfaces (Li et al., 2006; Sonka et al., 2015) is exceptionally well suited for the task. LOGISMOS identifies multiple interacting surfaces simultaneously, allows designing surface-and layer-specific cost functions reflecting both the surface-specific and regional (layer-specific) information, resulting surface shapes can be influenced by regionally varying surface smoothness and shape-preference constraints, and both the cost functions and constraints can be automatically learned from segmentation examples. Our LOGISMOS approach is now routinely used to simultaneously and computationally efficiently segment 11 intraretinal layers (12 surfaces) identified in Fig. 1 when applied to macular OCT scans, peripapillary OCT scans, or stitched multi-field OCT scans using a multi-scale 3-D graph search strategy (Fig. 1, https://www.iibi.uiowa.edu/content/shared-software-download). Another strength of the LOGISMOS approach is that it allows direct extension to 4-D and generally *n*-D images. An example of such a 4-D dataset may be a longitudinal sequence of 3-D OCT datasets, all of which can be segmented simultaneously by finding an optimal solution of a single graph-search problem. Additionally, the LOGISMOS approach allows highly efficient interactive modification of the resulting segmentations via our Just-Enough Interaction (JEI) strategy (Sun et al., 2013), in which an expert observer interacts with the underlying multi-surface segmentation algorithm by providing segmentation-correcting hints, in response to which graph costs are regionally modified and new optimal solutions found in real time (in milliseconds) by re-optimization of the underlying residual graph. This JEI approach, via interacting with the underlying graph-search algorithm inherently in 3D rather than correcting the surface tracings slice-by-slice allows to modify all segmentation surfaces simultaneously and with full consideration of spatial and multi-surface context, thus achieving very high efficiency of interactive surface segmentation result review and–if needed – their corrections. Once retinal layers are segmented (Haeker et al., 2006; Quellec et al., 2010; Bogunovic et al., 2014b), regional thickness, brightness, or texture-based indices of individual layers can be easily determined and thus contribute to our understanding of retinal or optic nerve head (ONH) disease processes and can be employed for determination of disease status, treatment responses, visual function, etc.

4. Quantitative analysis of the choroid

The choroid is a vascular bed located outside the retina and within the sclera with the highest blood flow of any tissue in the human body. The choroid is responsible for oxygenation and nourishment of the outer retina. The choroid consists of the choriocapillaris comprised of capillaries adjacent to Bruch's membrane and the choroidal proper with multiple layers that consists of larger vessels feeding or draining the choriocapillaris. The choroid is affected by many retinal diseases, its health reflected in choroidal or choriocapillary thickness may change in response to intravitreal drugs, and it also atrophies with age. Therefore, quantitative assessment of choroidal and choriocapillary thickness is of importance. We have developed a method for volumetric segmentation of choroidal vessels from standard OCT, allowing to derive local and regional thickness of the choroidal and choriocapillaris layers. The segmentation method starts with a segmented Bruch's membrane surface (Section 3) and uses a joint combination of the LOGISMOS (for surfaces) and graph-cut (for region) segmentation that uses spatially-contextual relationships to the previously segmented Bruch's membrane surface and simultaneously segments two surfaces (1–interface between the choroidal and choriocapillary layers, 2–the outer surface of the choroid) and the choroidal vascular bed (volumetric region), see Fig. 2. Note that the choroidal vasculature is segmented as a topologically-unconstrained region bounded by (mutually interacting with) the two surrounding surfaces. The choroidal vasculature and the two surrounding surfaces are segmented simultaneously in a single graph-based optimization process during which the vascular-region cost function is mainly based on locally-computed tubularity properties. Here, high cost values reflect presence of choroidal vessels. We have previously demonstrated that our approach is able to determine thinning of both the choroid and the choriocapillaris as a function of age (Zhang et al., 2012), as well as their thinning in response to frequent anti-VEGF injections that are used to treat the wet form of age-related macular degeneration (Almeida et al., 2014; Philip et al., 2016)].

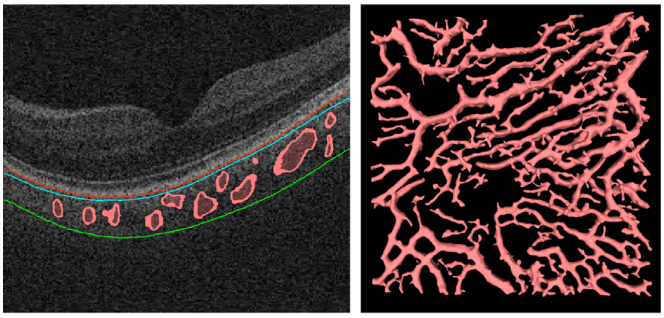

(a) (b)

Fig. 2. Choroidal segmentation. (a) Bruch's membrane, surface between the choriocapillaris and the choroidal plexus, and outlines of choroidal vessels shown on a B-mode slice. (b) Choroidal vasculature segmented in 3D.

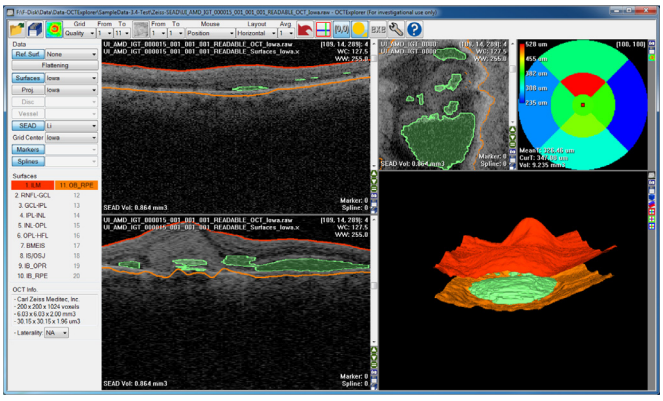

Fig. 3. Screenshot of OCT-Explorer environment–11 layer surfaces segmented (SEADs are shown in green). The upper right panels show an x-y (horizontal) slice cutting through the fluid region and the ability to perform regional analyses. The lower-right image shows a 3D visualization of the SEADs bounded by the ILM and RPE layer surfaces. (For interpretation of the references to colour in this figure legend, the reader is referred to the web version of this article.)

5. Image guided therapy in age-related macular degeneration

One of the greatest accomplishments of modern medicine is the transformation of choroidal neovascularization or CNV, the 'exudative' form of age related macular degeneration (AMD), from a disease with a poor visual outcome with essentially no effective treatment, to one where anti-VEGF agents allow most patients to retain useful vision. This has allowed millions of AMD patients around the world an improved quality of life. However, anti-VEGF treatments as currently administered have important disadvantages: They require frequent and expensive ($1,200–$24,000 per year) injections, often for life, these elderly patients have to be followed up frequently, each injection has a risk of devastating endophthalmitis, and long-term use of anti-VEGF agents may result in acceleration of another severe form of macular degeneration, geographic atrophy (Waldstein et al., 2016; Schmidt-Erfurth and Waldstein, 2016; Schlanitz et al., 2015). Various approaches have been attempted to minimize the number of injections by maximizing the interval between them. However, the recent results of the NIH-NEI funded CATT (Comparison of AMD Treatments Trials) and other studies show that visual outcomes at 2 years are inferior with fewer than monthly injections using current clinical decision approaches. The studies were always performed by retinal specialists and it is unknown whether general ophthalmologists would attain the same outcomes. For all these reasons, an objective patient-specific dosing strategy that allows the minimal necessary number of anti-VEGF injections while not decreasing visual outcomes is required and development of quantitative treatment-assistive strategies for these objective criteria is of utmost importance.

We have developed a combined strategy for quantitative analysis of 3D OCT retinal images, consisting of retinal layer segmentation, detection and quantification of retinal SEADs (symptomatic exudate-associated derangements), fluid, drusen, and pigment-epithelial detachments (PED's), the choroid, and choroidal vasculature in the presence of CNV pathology (Fig. 3) (Chen et al., 2012; Oguz et al., 2016). We have demonstrated that a patient-specific anti-VEGF treatment response can be predicted using a longitudinal OCT series of the treatment induction stage (initial 12 weeks of injections and OCT imaging) with promising accuracy (Fig. 4a) (Bogunovic et al., 2014a). When focusing on prediction of patient's total retinal thickness (TRT) and visual acuity (VA) from a longitudinal OCT series of OCT data, a predicted TRT 4 weeks and VA 12 weeks after the end of the induction phase correlated well with the measured values ($R = 0.77$ in 65 patients and $R = 0.57$ in 47 patients, Fig. 4b and c).

6. Determination of visual function from retinal morphology

Glaucoma is a progressive disease of the optic nerve and, if left untreated, can lead to irreversible loss of vision. Glaucoma results in apoptosis of the retinal ganglion cells (RGCs) with corresponding nerve fiber loss (Hood et al., 2007, 2008; Wheat et al., 2012). The disease effect on multiple neighboring ganglion cells and corresponding axons leads to regional visual field loss, optic nerve head cupping, and the disease manifestation is distributed along the entire length of the Retinal-Ganglion-Cell Axonal complex (RGC-AC). Glaucoma needs to be detected early, and once detected, changes in glaucomatous damage must be consistently monitored. Automated perime-try (e.g., Humphrey 24-2 SITA visual field), and clinical assessment of the optic nerve cup and rim are the main clinical standard for detection of glaucoma and its progression. Unfortunately, even for moderate visual field (VF) loss (exceeding 12–15 dB mean deviation loss), VF measurement variability increases and a reliable determination of VF change is not possible. This lack of reliability and reproducibility of VF measurement, in addition to its patient unfriendliness is problematic in glaucoma damage assessment.

Using our previously validated SD-OCT segmentation and registration of methods (Section 3), registration of 9-field OCT covering all of the Humphrey 24-2 visual field test locations allows precise quantification of local GCL and NFL thickness at each of the 54 VF-test locations. Combined with the RGC-AC concept and its axonal trajectory according to Garway–Heath, these analysis techniques allow aggregate glaucoma damage as-sessment for each RGC-AC complex. On a grid coinciding with the 54 cell locations of the Humphrey 24-2 visual testing, independent predictive models are built for each cell. Each cell-specific predictive model is based on the structural properties of the associated RGC-AC that originates at the cell of interest. Thus, the properties are composed of the average cell thickness of the GCL+IPL layer, the average NFL thickness over the cell, as well as the NFL thicknesses of all the cells along the estimated RGC-AC. The cell-specific predictive models were implemented as a support vector regression machine and trained using these features to predict the continuous out-put represented by the VF threshold for each of the 54 cells. Example predictions obtained from a set of 54 independently trained predictive models are given in Fig. 5. When quantitatively comparing the actual VF thresholds from Humphrey VF to the thresholds derived from the RGC-AC based cell-specific predictive models, the correlation

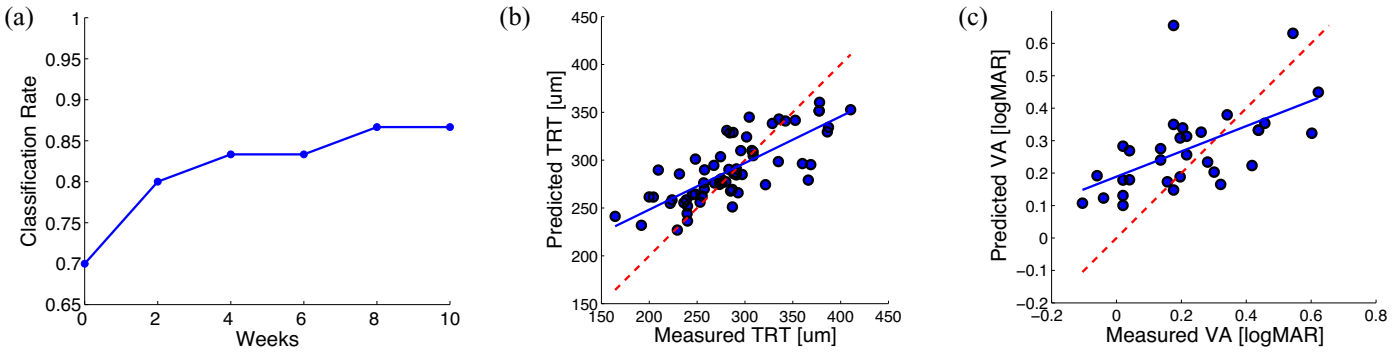

Fig. 4. Prediction of patient-specific outcomes. (a) Prediction correctness as a function of adding more and more data from the induction phase–note that 83% correctness is achieved after only 4 weeks of the induction period. (b) Prediction of total retinal thickness (TRT) with correlation coefficient $R = 0.77$ ($p < 0.001$). (c) Prediction of visual acuity (VA) with correlation coefficient $R = 0.57$ ($p < 0.001$). Corresponding regression lines (in panels b,c) are in blue. The identity line is shown in red. (For interpretation of the references to colour in this figure legend, the reader is referred to the web version of this article.)

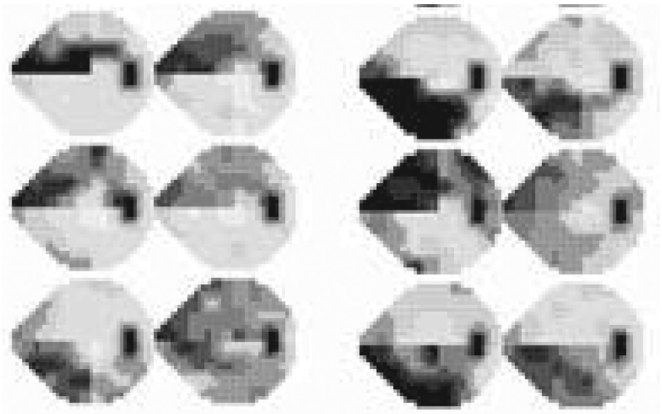

Fig. 5. Visual fields presented as simulated Humphrey 24-2 VF test printouts. The actual perimetry measured thresholds are shown on the left of each pair, the predicted VF threshold is shown on the right. The left column of paired VF printouts corresponds to moderate glaucoma and the right pair to advanced glaucoma. Note that the predictions correspond quite well with the measured VF data in this randomly selected small subset of 122 analyzed eyes with early, moderate, and advanced glaucoma.

across the VF grid cells ranged from 0.48 to 0.81, with a mean of 0.68 (Bogunovic et al., 2015).

The presented ability to predict visual function from retinal layer structure derived from volumetric OCT may potentially be game-changing for patients with glaucoma and possibly with other vision-loss causing retinal diseases. Visual field assessment is a demanding test that requires focused and active attention of the tested patient for 20–30 min. In comparison, a volumetric OCT scan only takes about a minute of passive participation. Therefore, the increased reproducibility of the VF determination, as well as the potential of replacing the unpopular visual field test with a single volumetric OCT imaging session will allow to test glaucoma patients more frequently, more reproducibly, and thus detect glaucoma earlier. It also promises to achieve a better understanding of the patient-specific disease process that will allow to administer patient-specific treatment.

7. Discussion and conclusion

The previous sections show how quantification applied to standard OCT protocols is starting to affect clinical practice for patients with ocular diseases. From here, there are three future directions for quantitative OCT. First, to achieve earlier detection of treatable diseases, also called screening, OCT and OCT analysis will need to be adapted to use in frontline care. This implies a shift to diagnostic rather than quantification performance, as well as lower cost hardware, such as snapshot OCT. Second, as we have shown in the glaucoma studies and other studies not discussed here, OCT analysis has the potential to replace the mainstay of disease management in ophthalmology, namely functional tests. For example, replacing visual field thresholds with OCT analysis, replacing contrast sensitivity or dark adaptation with OCT analysis, etc. All of these traditional tests are patient unfriendly and are plagued by low reproducibility, while smart OCT analysis has the potential to make these into quick, easy tests for patients and doctors alike. Third, increasing resolution of OCT hardware to that beyond cellular resolution, e.g., via adaptive optics OCT (resolution is increased by correcting for waveform aberrations resulting from the imperfections in the ocular media) or using contrast-enhanced OCT (both these approaches now feasible only in a research setting) will necessitate even faster and more precise quantification algorithms.

Acknowledgment

This work was supported, in part, by NIH grants R01 EY019112, R01 EY018853 and R01 EB004640; the Depart ment of Veterans Aff airs; the Arnold and Mabel Beckman Initiative for Macular Research (BIMR) #18350500; and the Christian Doppler Society OPTIMA project. We gratefully acknowledge the contribution of our colleagues to many aspects of the research presented here, namely Drs. Young Kwon, Hrvoje Bogunovic, Xinjian Chen, Kyungmoo Lee, Ipek Oguz, Andreas Wahle, and Li Zhang.

References

Abràmoff, M.D., Garvin, M.K., Sonka, M., 2010. Retinal imaging and image analysis. IEEE Rev. Biomed. Eng. 3, 169–208.

Almeida, D., Zhang, L., Chin, E.K., Mullins, R.F., Kucukevcilioglu, M., Critser, D.B., Sonka, M., Stone, E.M., Folk, J.C., Abràmoff, M.D., et al., 2014. Comparison of retinal and choriocapillaris thicknesses fol-lowing sitting to supine transition in healthy individuals and patients with age-related macular degeneration. JAMA Ophthalmol. in print.

Bogunovic, H., Abramoff, M., Zhang, L., Sonka, M., 2014a. Prediction of treatment response from retinal OCT in patients with exudative age-related macular degeneration. In: Chen, X., Garvin, M.K., Liu, J.J. (Eds.), Proceedings of the Ophthalmic Medical Image Analysis First International Workshop, OMIA 2014. Boston, MA, pp. 129–136.

Bogunovic, H., Kwon, Y., Rashid, A., Lee, K., Critser, D., Garvin, M., Sonka, M., Abramoff, M., 2015. Relationships of retinal structure and Humphrey 24-2 visual field thresholds in patients with glaucomaretinal structure and Humphrey 24-2 visual field. Invest. Ophthalmol. Visual Sci. 56, 259.

Bogunovic, H., Sonka, M., Kwon, Y.H., Kemp, P., Abràmoff, M.D., Wu, X., 2014b. Multi-surface and multi-field co-segmentation of 3-D retinal optical coherence tomography. IEEE Trans. Med. Imaging 33 (12), 2242–2253.

Chen, X., Niemeijer, M., Zhang, L., Lee, K., Abramoff, M.D., Sonka, M., 2012. Three-dimensional segmentation of fluid-associated abnormalities in retinal OCT: probability constrained graph-search-graph-cut. IEEE Trans Med Imaging 31 (8), 1521–1531.

Geitzenauer, W., Hitzenberger, C.K., Schmidt-Erfurth, U.M., 2011. Retinal optical coherence tomography: past, present and future perspectives. Br. J. Ophthalmol. 95 (Feb(2)), 171–177.

Haeker, M., Abràmoff, M., Kardon, R., Sonka, M., Jan. 2006. Segmentation of the surfaces of the retinal layer from OCT images. In: Medical Image Computing and Computer-Assisted Intervention (MICCAI) 2006, 4190. Springer-Verlag, pp. 800–807.

Hood, D.C., Anderson, S., Rouleau, J., Wenick, A.S., Grover, L.K., Behrens, M.M., Odel, J.G., Lee, A.G., Kardon, R.H., 2008. Retinal nerve fiber structure versus visual field function in patients with ischemic optic neuropathy. A test of a linear model. Ophthalmology 115 (May(5)), 904–910.

Hood, D.C., Anderson, S.C., Wall, M., Kardon, R.H., 2007. Structure versus function in glaucoma: an application of a linear model. Invest. Ophthalmol. Vis. Sci. 48 (8), 3662–3668.

Li, K., Wu, X., Chen, D.Z., Sonka, M., 2006. Optimal surface segmentation in volumetric images — A graph-theoretic approach. IEEE Trans. Pattern Anal. Mach. Intell. 28, 119–134.

Oguz, I., Zhang, L., Abramoff, M.D., Sonka, M., 2016. Optimal retinal cyst segmentation from OCT images. In: Proceedings of the SPIE 9784, Medical Imaging 2016: Image Processing. SPIE, Bellingham, WA, p. doi:10.1117/12.2217355.

Philip, A.M., Gerendas, B.S., Zhang, L., Faatz, H., Podkowinski, D., Bogunovic, H., Abramoff, M.D., Hagmann, M., Leitner, R., Simader, C., Sonka, M., Waldstein, S.M., Schmidt-Erfurth, U., 2016. Choroidal thickness maps from spectral domain and swept source optical coherence tomography: algorithmic versus ground truth annotation. Br. J. Ophthalmol. (Jan) doi:10.1136/bjophthalmol-2015-307985.

Quellec, G., Lee, K., Dolejsi, M., Garvin, M.K., Abràmoff, M.D., Sonka, M., 2010. Three-dimensional analysis of retinal layer texture: identification of fluid–filled regions in SD-OCT of the macula. IEEE Trans Med Imaging 29 (Jun(6)), 1321–1330.

Schlanitz, F.G., Sacu, S., Baumann, B., Bolz, M., Platzer, M., Pircher, M., Hitzenberger, C.K., Schmidt-Erfurth, U., 2015. Identification of Drusen characteristics in age-related macular degeneration by polarization-sensitive optical coherence tomography. Am. J. Ophthalmol. 160 (Aug(2)), 335–344.

Schmidt-Erfurth, U., Waldstein, S.M., 2016. A paradigm shift in imaging biomarkers in neovascular age-related macular degeneration. Prog. Retin Eye Res. 50 (Jan), 1–24.

Sonka, M., Hlavac, V., Boyle, R., 2015. Image Processing, Analysis, and Machine Vision, Fourth ed. Cengage Learning, Toronto, Canada (1st edition Chapman and Hall, London, 1993; 2nd edition PWS Pacific Grove, CA, 1997, 3rd edition Thomson Engineering, 2008).

Sun, S., Sonka, M., Beichel, R.R., 2013. Graph-based IVUS segmentation with efficient computer-aided refinement. IEEE Trans. Med. Imaging 32 (8), 1536–1549.

Waldstein, S.M., Wright, J., Warburton, J., Margaron, P., Simader, C., Schmidt-Erfurth, U., 2016. Predictive value of retinal morphology for visual acuity outcomes of different Ranibizumab treatment regimens for neo-vascular AMD. Ophthalmology 123 (Jan(1)), 60–69.

Wheat, J.L., Rangaswamy, N.V., Harwerth, R.S., 2012. Correlating RNFL thickness by OCT with perimetric sensitivity in glaucoma patients. J Glaucoma 21, 95–101.

Zhang, L., Lee, K., Niemeijer, M., Mullins, R., Sonka, M., Abramoff, M., 2012. Automated segmentation of the choroid from clinical SD-OCT. Invest. Ophthalmol. Vis. Sci. 53, 75107519.